AIAA JOURNAL
Vol. 39, No. 1, January 2001

Surface Pressure Measurements of the Orthogonal Vortex Interaction

C. J. Doolan,* F. N. Coton,† and R. A. M. Galbraith‡
University of Glasgow, Glasgow, Scotland G12 8QQ, United Kingdom

A unique vortex generator that simulates the trailing vortex produced by a helicopter main rotor in forward flight was used in a study of main rotor/tail rotor blade vortex interaction. Velocity measurements were performed using hot wire anemometry and particle image velocimetry, which showed the interacting vortices to be three dimensional and to contain a significant core axial flow. Surface pressure measurements during vortex collision with an instrumented, stationary blade were obtained at a variety of incidence settings. At the leading edge, a suction peak occurred where the core flow was directed away from the surface and, similarly, a pressure peak occurred where the core flow was directed toward the surface. This behavior can be explained in terms of the impulsively blocked vortex core axial flow. Also, the leading edge suction and pressure peaks were amplified or attenuated by changing the incidence of the blade. However, the changes in surface pressure distribution were such that the peak normal force was approximately the same for each incidence setting.

Nomenclature

C_m = quarter chord pitching moment coefficient, $M/\frac{1}{2}\rho V_\infty^2 c^2$
C_n = normal force coefficient, $F/\frac{1}{2}\rho V_\infty^2 c$
C_p = pressure coefficient, $(p - p_\infty)/\frac{1}{2}\rho V_\infty^2$
c = interacting blade chord, m
c_R = rotor blade chord, m
F = normal force per unit span, Nm^{-1}
M = quarter chord pitching moment per unit span, N
R = rotor radius, m
r_c = vortex core radius, m
s = distance along path enclosing vortex core, m
t = time, s
u = velocity component aligned with freestream, ms^{-1}
V = velocity, ms^{-1}
v = vertical velocity, ms^{-1}
W = vortex core velocity, ms^{-1}
w = cross-stream velocity, ms^{-1}
x = distance, m
α = angle of incidence, deg
Γ = circulation, $\mathrm{m}^2\mathrm{s}^{-1}$
ν = kinematic viscosity, $\mathrm{m}^2\mathrm{s}^{-1}$
ρ = freestream density, kgm^{-3}
Ω = rotation velocity of rotor, rads^{-1}

Subscripts

s = time-averaged measurement
u = measurement made during interaction
∞ = freestream conditions
θ = tangential

Introduction

BLADE vortex interactions (BVI) in rotorcraft are a well-known source of unwanted noise and vibration. They are caused when the trailing vortex from a main rotor blade encounters another blade on the aircraft. Much research has been performed for the case of main rotor BVI where the vortex interacts with another main rotor blade.[1,2] Less is known about the orthogonal interaction of this vortex and a tail rotor blade in the manner depicted in Fig. 1. If the thickness of the leading edge is sufficiently small, the vortex is severed or cut as it collides with the blade. It should also be pointed out that similar BVI may occur in the compressor cascades of turbomachinery.[3]

Previous research into the orthogonal vortex interaction has included mathematical and experimental studies. Analytical investigations have been performed by Howe[4] and Marshall.[5] Computational investigations using different numerical approaches[6–8] show that the vortex dynamics during cutting are controlled by the axial flow within the vortex core. If the axial flow is directed toward the cutting surface, the core bulges, and if the axial flow is away from the surface, the core thins.

Flow visualizations of the vortex cutting process[8–10] verify the core bulging and thinning and also show the production of secondary vorticity and entrainment of the blade boundary layer into the core. Surface pressure and noise measurements of the orthogonal vortex interaction[11,12] show a difference in pressure measurements on either side of the cutting surface, which could possibly be due to an axial core component. Although these studies are important, in the published data, it is difficult to resolve the instantaneous surface pressures over the entire chord during vortex cutting. Also, the experimental apparatus in previous research produce vortices that are representative of the wake of a hovering rotor or propeller rather than a helicopter in forward flight. Recently, surface pressure measurements of the orthogonal interaction have been performed.[13] In this work, only the basic orthogonal interaction with a blade at zero incidence is reported. Results show the effect of the vortex impacting the leading edge at two different approach angles. Also, only minimal vortex information can be related to the pressure data.

In the present paper, detailed results of a series of experiments investigating the orthogonal vortex interaction are presented. First, velocity measurements of the three-dimensional vortex used for the interaction tests are shown. Measurements were obtained using hot-wire anemometry and particle image velocimetry (PIV). An instrumented blade was then placed in the path of the vortex to collect surface pressures during the vortex interaction. This blade was placed at different angles of incidence to examine what changes this imposed on blade loading during the interaction. The surface pressure measurements were also integrated around the chord to yield transient normal force and quarter chord pitching moment (per unit span) data. The integrated records are presented to show the effect of blade incidence and are related to the velocity measurements of the three-dimensional vortex.

Experiment

The experiments were conducted in the Glasgow University 1.15×0.85 m low-speed wind tunnel. This is a closed-return facility with a working section length of 1.8 m and is capable of

Received 4 October 1999; revision received 11 February 2000; accepted for publication 7 April 2000.

*Postdoctural Research Assistant, Department of Aerospace Engineering. Member AIAA.
†Senior Lecturer, Department of Aerospace Engineering. Member AIAA.
‡Professor, Department of Aerospace Engineering. Member AIAA.

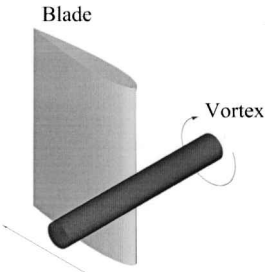

Fig. 1 Illustration of orthogonal vortex interaction.

speeds up to 33 m/s. During testing, the freestream velocity and temperature were monitored continuously using a pitot-static tube and thermocouple device located in the working section.

The design of the vortex generator has been previously detailed by Copland[14] but will, for convenience, be summarized here. The vortex generator is essentially a rotor of radius 0.75 m that has a single rectangular planform blade of chord 0.1 m with a NACA 0015 cross section. During rotation, the blade pitch is varied using a spring-loaded pitch link running on a cylindrical cam configured such that the blade pitch varies in four equivalent (90 deg) phases of azimuth. The first phase sets the blade at zero incidence while the blade is pointing into the settling chamber (45-deg azimuthal travel on either side of the wind tunnel center line). In the next two phases of motion, the blade is pitched from 0 to 10 deg, before traversing the working section at a constant 10-deg incidence. In the final 90-deg phase, the spring-loaded pitch link forces the blade to overcome its aerodynamic and inertial loads and follow the cam as it returns to 0 deg.

The rotor assembly is mounted on a vertical rotating shaft supported by bearings installed in an external framework above and below the wind tunnel contraction. Also located on this framework is a DC electric motor used to drive the rig. During operation, the rotational speed is monitored by an optical sensor located on the main shaft.

Velocity measurements of the convecting vortex were made using a TSI IFA-300 hot-wire annemometer system using DANTEC 55P61 cross-wire probes. The probes used 5-μm-diam, platinum-plated tungsten wires with a length-to-diameter ratio of 250. The measuring volume of the probe was approximately 0.8 mm in diameter and 0.5 mm in height.

The probe was calibrated in a special wind tunnel dedicated to the purpose. During calibration, the probe was rotated (in 6-deg steps) ± 30 deg in the plane of the sensor wires to determine yaw sensitivity. A full account of the calibration procedures used can be found in Ref. 14. Data were recorded at 10 kHz in 2048 sample blocks.

Independent velocity measurements were also made using a PIV system, which uses a Spectra-Physics Nd:YAG laser operating in a double-pulsemode with 50-μs separation. The flow was seeded with 1–2-μm oil smoke particles distributed throughout the flow. The laser light was passed through an optical arrangement that converted the beam into a laser sheet that was passed through the working section to illuminate the flow seeding. The particle displacements could then be recorded using a Kodak Megaplus ES 1.0 camera of 1k $\times$ 1k resolution. A cross correlation routine then determined the velocity vectors within the illuminated region.[15]

The vortex generator produces a curved, three-dimensional vortex that convects through the wind-tunnel working section. A NACA 0015 blade of chord 152.4 mm and overall span 944 mm was placed in the path of the convecting vortex to study the interaction of the vortex with the blade. The experimental setup allowed a variation of the geometric incidence of the blade. Measurements were obtained within a blade incidence range of ± 10 deg using 2-deg increments. When set at 0 deg, the leading edge of the blade was 2000 mm or 13.12 blade chord lengths downstream of the rotor center line. The blade was instrumented at 78.5% span with a chordal array of 30 miniature Kulite pressure transducers mounted around the surface of the blade. The transducers were connected to a surface orifice of 1-mm diam.

For the current test program the freestream velocity was fixed at 20 m/s and the rotational speed of the vortex generator was 500 rpm.

Table 1 Maximum blade tip nondimensional operating parameters

Parameter	Value
Tip Mach number	0.18
Tip Reynolds number	3.95×10^5
Tip vortex strength ($\Gamma / R\Omega c_R$)	0.47
Tip vortex reynolds number (Γ / ν)	1.3×10^5

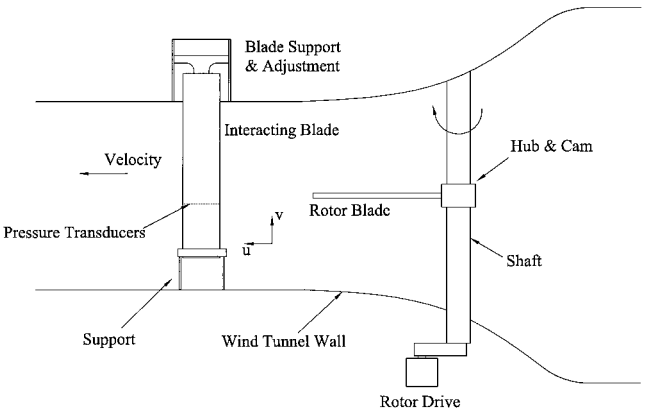

Fig. 2 Schematic showing vortex generator and interacting blade.

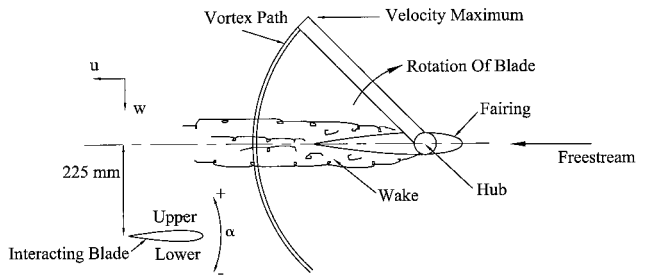

Fig. 3 Plan view of wind tunnel showing interacting blade position.

These settings had been previously identified by Doolan et al.[16] to provide a clear, well-defined, tip vortex structure in the working section. Based on these conditions, the nominal interacting blade Reynolds number was 2×10^5. Operating parameters for the transverse vortex generator are displayed in Table 1 and were determined using a numerical procedure outlined in Ref. 13.

As shown schematically in Fig. 2, the blade was mounted from the roof of the working section and extended to the tunnel floor. To facilitate the change in incidence of the blade, a specially designed support was located on the tunnel floor. Also, the blade was placed 225 mm from the tunnel centerline (Fig. 3) to avoid the turbulent wake of the vortex-generator support shaft. Previous velocity measurements have shown that the vortex is obscured by this wake.[16]

The approach angle between the convecting vortex and instrumented blade at $\alpha = 0$ deg was calculated using a free-wake model of the trailing vortex and a source-panel representation of the wind-tunnel walls.[16] Hot-wire measurements were used to verify the free-wake model results,[16] and the experimental uncertainty was calculated to be ± 5 deg. Therefore, the uncertainity in the approach angle can be considered to be ± 5 deg. The height of the instrumented blade was set such that the chordwise transducers were positioned in the path of the vortex core. This position was determined using the results of a hot-wire probe survey.

Pressure data for each transducer were recorded using a BE256 data logger in a single 32,000-sample block at a 20-kHz sampling rate. This sample rate and size allowed approximately 13 rotor revolutions of data capture. Five blocks of data were obtained at each blade incidence.

The BE256 data logger and software employs an automatic gain adjustment feature that allows measurements to be taken at the maximum resolution possible for the system. On the basis of previous experience with the Kulite miniature transducers[2] and taking account of discretization and calibration factor errors, the uncertainty in the measured pressure coefficient was estimated at 0.5%. Using a technique similar to that of Baines et al.,[17] the maximum uncertainty in the force and pitching moment coefficients was estimated to be 2.1%.

The largest source of error in the measurements was vortex position. Once produced by the rotor rig, the vortex is free to convect through the wind tunnel. Each successive vortex follows a slightly different path due to variations in local conditions about the rotor blade and freestream turbulence levels. Using hot-wire measurements of the vortex dimensions and a numerical procedure, the wandering amplitude of the vortices has been estimated to be 19% of the interacting blade chord.[16] The wandering imparts uncertainty regarding the location of the vortex relative to the transducer array. Accordingly, 65 interactions were recorded at each test position and representative data sets were extracted at the quoted transducer locations.

Results and Discussion

Vortex Velocity Measurements

Hot-wire velocity measurements were taken at the position of the instrumented blade leading edge prior to the installation of the blade. During the test, the probe was traversed vertically through the working section, and the transient vortex velocity field was acquired. The height of vortex core passage was considered to be the position where, on average, the maximum vertical velocity signal v was recorded. (It is directly related to the vortex tangential velocity through a simple transformation.[16]) The blade was then installed, and so the transducers were placed at this height and, therefore, in the path of the vortex core.

Hot-wire velocity measurements obtained at the vortex passage height are presented in Fig. 4. The results in Fig. 4 were obtained in two tests with the probe in the same position in space but in two different orientations separated by a 90-deg rotation about the probe axis. This was necessary to allow a single probe to measure both vertical and cross-stream velocities. In Fig. 4a, the vertical velocity data show an induced velocity field characteristic of a rotor trailing vortex system. The variation between successive vortices is due to vortex wandering and local turbulence levels. The cross-stream velocity component is shown in Fig. 4b and, during vortex passage over the probe, represents the flow along the core of the vortex. A significant cross-stream velocity was measured, which suggests the presence of a vortex core axial flow. When the model is installed in the wind tunnel, the direction of the core flow is toward the lower surface and away from the upper surface.

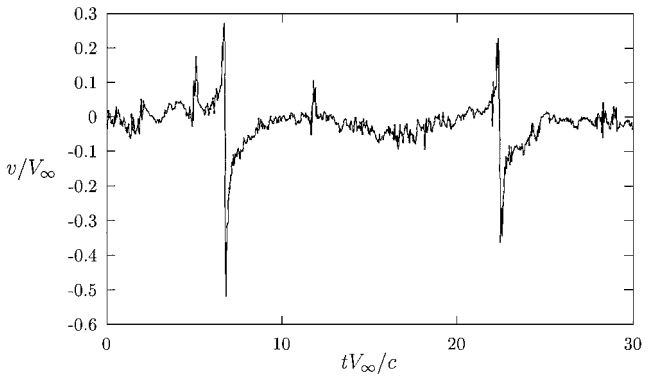

a) Vertical velocity record

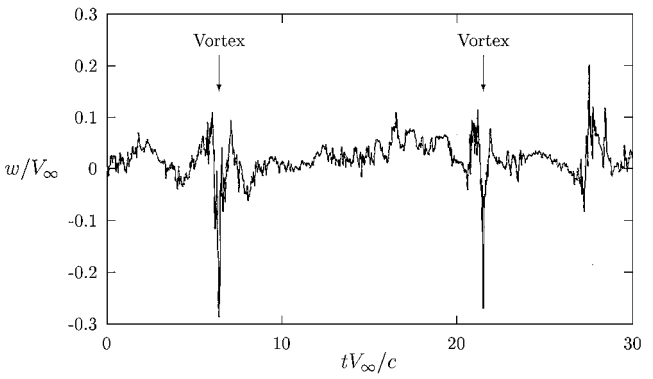

b) Cross-stream velocity record

Fig. 4 Velocity measurements at blade leading edge location.

The measured axial core velocity may originate from two sources. The first is essentially a viscous momentum loss phenomenon, usually associated with the core region of fixed-wing trailing vortices and wakes of bluff bodies. This type of axial flow was measured by Han et al.[18] in the core of the trailing vortex from a hovering rotor blade. It was found that, in this case, the core axial flow diminished rather quickly with wake age. The second mechanism for the generation of axial flow is an induced pressure gradient due to nonuniform vortex strength along the core. The rotor tip experiences a continually changing velocity field because of the generation of a combination of tunnel freestream and rotational velocity components similar to that generated by the rotor blades of a helicopter in forward flight. Circulation strength is therefore expected to vary along the core, which would produce an axial pressure gradient and associated velocity directed along the core.

PIV was also used to verify the position of the vortex and to quantify the total circulation about the core. A relatively high rotational velocity gradient exists within the vortex core, which subjects entrained smoke particles to high centripetal and coriolis accelerations. Any particles initially within the core follow a spiral path that ejects them into the surrounding fluid.[19] This was noticed as a dramatic drop in seed particle density within the vortex-core region. Hence, the PIV system has poor resolution of the velocities within the core.

Table 2 Summary of vortex parameters

Parameter	Value
r_c/c	0.065 ± 0.031
$\Gamma/\Omega R c_R$ (PIV)	0.144 ± 0.022
$\Gamma/\Omega R c_R$ (hot wire)	0.120 ± 0.044
W/V_∞	0.4 ± 0.12

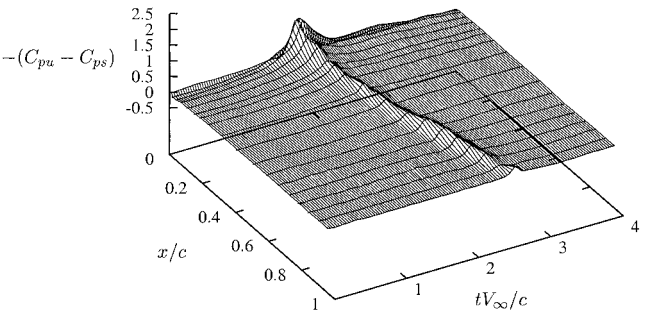

a) Upper surface

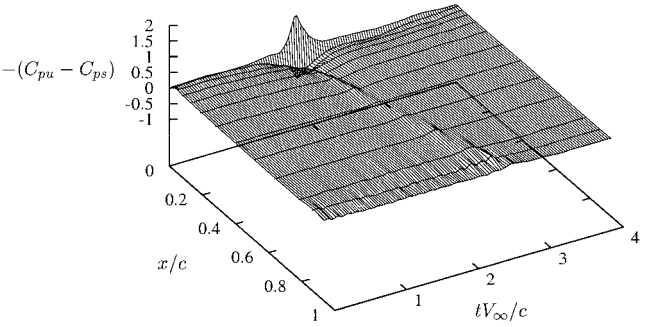

b) Lower surface

Fig. 5 Unsteady pressure measurements on blade surface; $\alpha = 0$ deg.

The PIV measurements are therefore more useful for measuring the total circulation of the vortex rather than information within the core. Because it is a global measurement system, a particular region of the flowfield can be analyzed, rather than a particular point in space, which is the case for a probe-based measurement technique. Therefore, errors induced in the circulation measurements by vortex wandering in probe-based techniques can be reduced by using PIV and sampling a region larger than the wandering amplitude of the vortex. Although methods exist that can correct hot-wire velocity measurements for wandering effects (e.g., Ref. 20), the wandering amplitude in this case is too large for them to be applied. By integrating the tangential velocity about the edges of a region several core diameters away from the vortex core, an estimate of the total circulation can be made. The integral,

$$\Gamma = \oint V_\theta \, \mathrm{d}s \tag{1}$$

was evaluated, where $\mathrm{d}s$ is a small portion of a path enclosing the vortex core. The actual path chosen was the edge of the analyzed image, with the vortex approximately in the center and $\mathrm{d}s = 2.5$ mm. A first-order approximation for the integral was used.

A summary of the vortex parameters can be found in Table 2. The hot-wire results were used to obtain estimates of the vortex core size. This is defined as the distance between the peak tangential

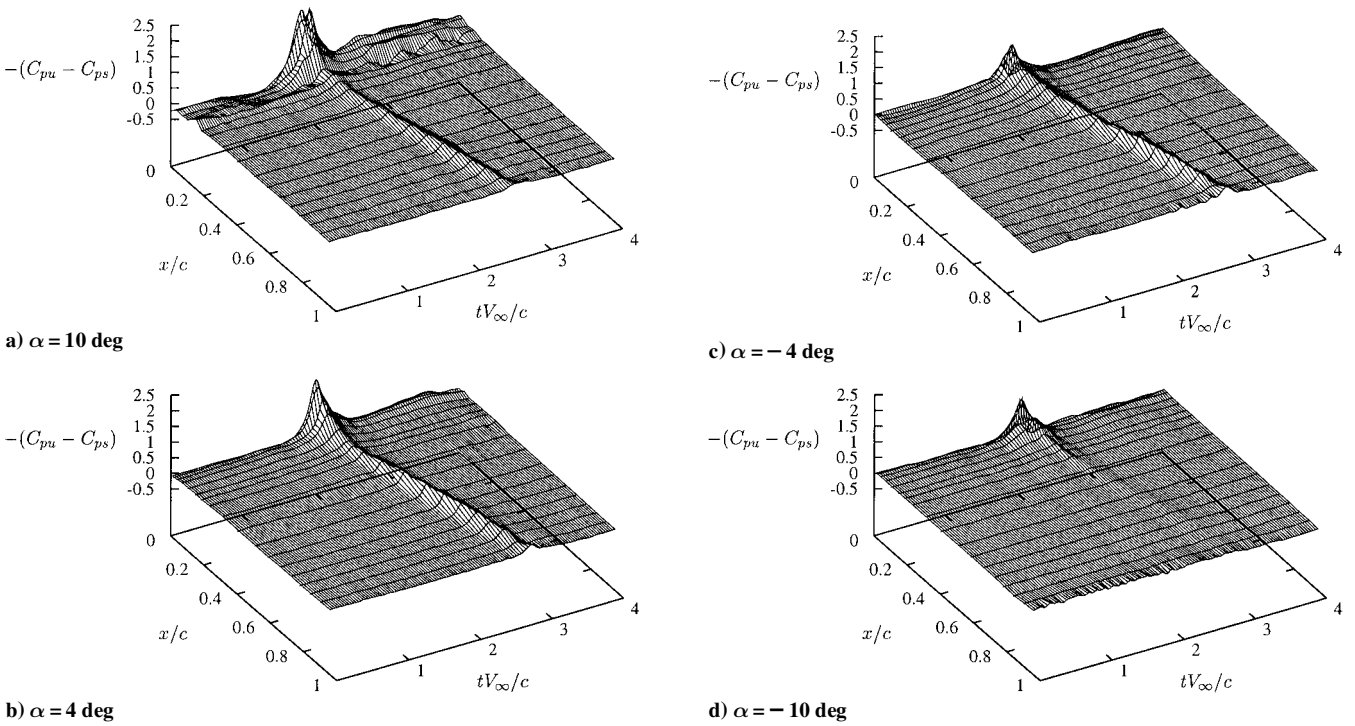

a) $\alpha = 10$ deg **c) $\alpha = -4$ deg**

b) $\alpha = 4$ deg **d) $\alpha = -10$ deg**

Fig. 6 Unsteady pressure measurements on upper surface of loaded blade.

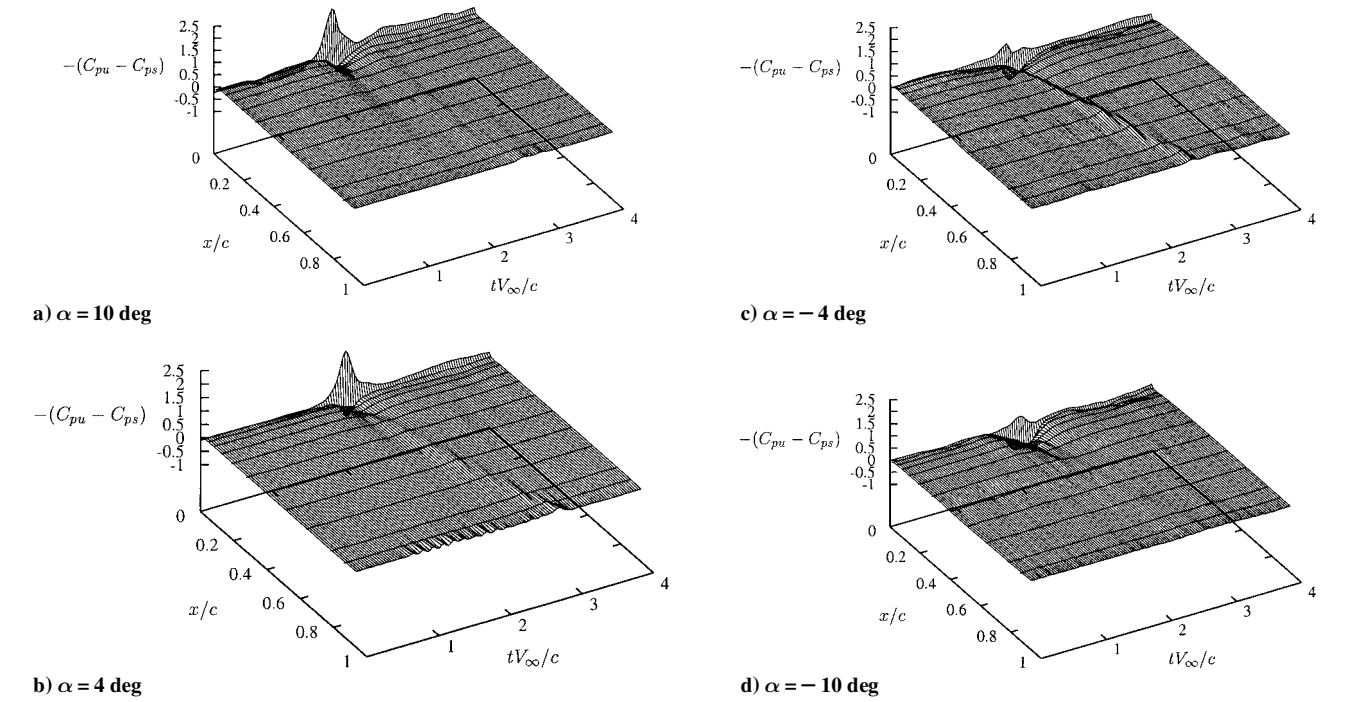

a) $\alpha = 10$ deg **c) $\alpha = -4$ deg**

b) $\alpha = 4$ deg **d) $\alpha = -10$ deg**

Fig. 7 Unsteady pressure measurements on lower surface of loaded blade.

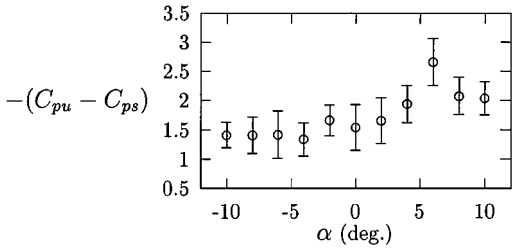

Fig. 8 Peak suction recorded during orthogonal interaction on upper surface for transducer placed at *x/c* = 0.009.

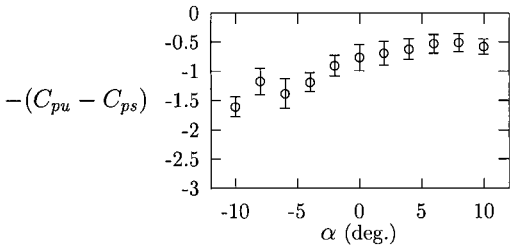

Fig. 9 Peak pressure recorded during orthogonal interaction on lower surface for transducer placed at *x/c* = 0.011.

velocities on a line passing through the vortex center. The PIV measurements were used to obtain the vortex circulation. The hot-wire measurements were also used to obtain circulation measurements and the differences are indicated in Table 2. The benefits of using the PIV system are obvious, with the uncertainty in the measurements reduced by 50%. The uncertainty was calculated by taking the standard deviation of 10 vortex results.

The vortex information presented was used to estimate the blade impact parameter ($2\pi r_c V_\infty / \Gamma = 2.16$) and the axial flow parameter ($2\pi r_c W / \Gamma = 0.89$). These dimensionless parameters have been identified by Marshall and Krisnamoorthy[8] as quantities that indicate the severity of the physical response to the vortex cut. The obtained value of the blade impact parameter implies a weak interaction, with no boundary-layer separation, before the vortex collides with the leading edge. It has been shown by Krisnamoorthy and Marshall[9] that the weak vortex interaction is the dominant tail-rotor interaction mechanism for a helicopter in forward flight with an advance ratio greater than approximately 0.1.

The value of the axial flow parameter determines some aspects of the vortex dynamics during a vortex cut. For these experiments, the value reported indicates that the vortex is supercritical and only downstream-area waves of small amplitude can be supported on the vortex core.[8] If a supercritical vortex hits the instrumented blade, a jetlike flow occurs on its lower surface while a thinning of the vortex core occurs on the upper surface.

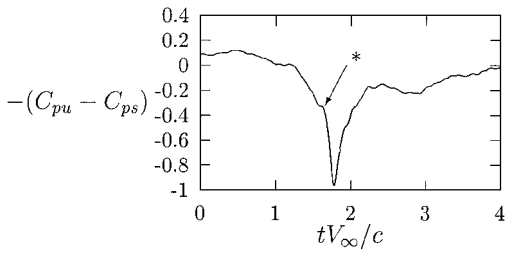

a) *x/c* = 0.011

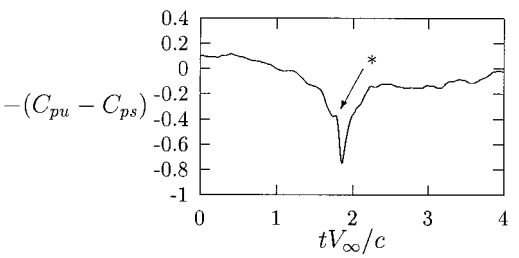

b) *x/c* = 0.037

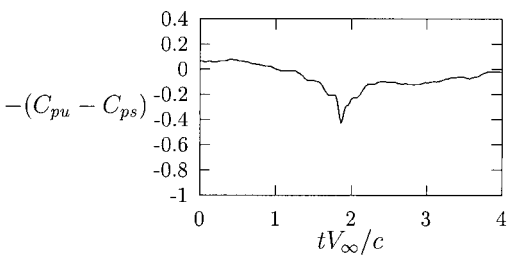

c) *x/c* = 0.069

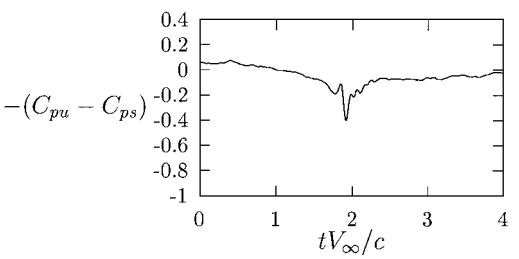

d) *x/c* = 0.118

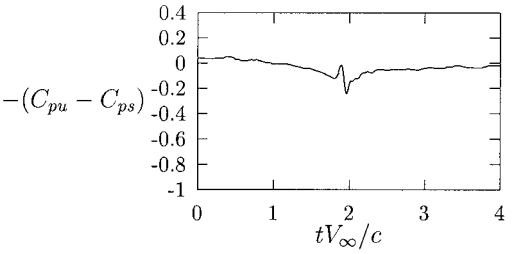

e) *x/c* = 0.183

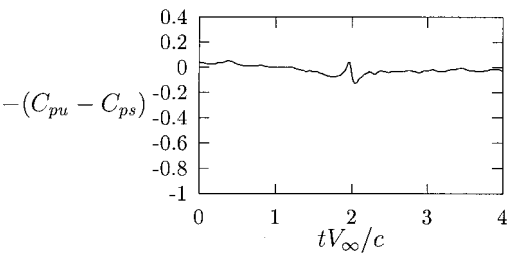

f) *x/c* = 0.276

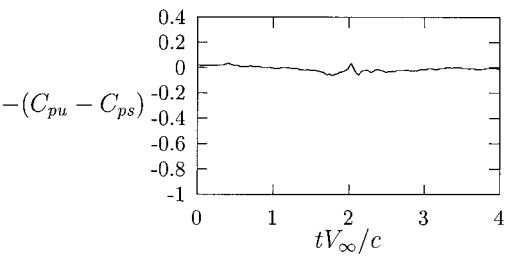

g) *x/c* = 0.387

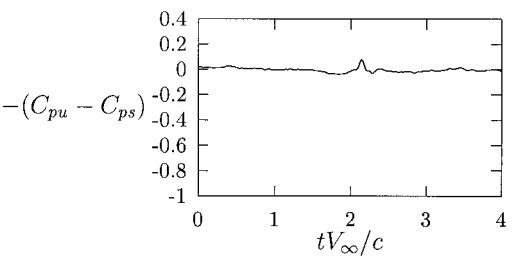

h) *x/c* = 0.502

Fig. 10 Transient pressure records on lower surface; $\alpha = 0$ deg.

Orthogonal Interaction Tests

The upper and lower surfaces of the blade are defined in Fig. 3, as are the directions of positive and negative blade incidence.

Figure 5 illustrates the temporal variation of the pressure data recorded as the vortex is cut by a blade set at zero incidence. In each plot, the time-averaged component of the pressure signal has been removed to increase the clarity of the results. The time-averaged component C_{ps} was determined by averaging the 32,000 pressure samples obtained during each test. Hence, $-(C_{pu} - C_{ps})$ is plotted on the vertical axis with the chord position of the transducers (x/c) on one axis and nondimensional time tV_∞/c on the foreground axis. To further increase the clarity of the plots, only every fifth data sample is presented.

The upper-surface interaction data in Fig. 5a show a strong suction peak at the leading edge when the vortex first encounters the blade. As the vortex passes over the surface, this suction peak diminishes but remains prominent over the rest of the chord.

For the lower surface (Fig. 5b), an increase in pressure occurs just downstream of the leading edge. At approximately 15% chord, the pressure ridge transforms into a slight suction ridge that convects over the blade. For all lower surface plots, the leading edge pressure record is repeated for completeness.

Results of the vortex interaction with a loaded blade for a selection of incidence settings are shown in Figs. 6 and 7. On the upper surface, the suction peak at the leading edge is seen to intensify when the blade is set at positive incidence (Figs. 6a and 6b) and reduce somewhat at negative incidence (Figs. 6c and 6d). This effect can be observed in more detail in Fig. 8, where peak suction measurements obtained during the interaction from the transducer placed at $x/c = 0.009$ are plotted against blade incidence. Each data point represents an average of 20 interactions, and the error bars indicate one standard deviation either side of the mean. Despite a significant scatter, thought to be due to vortex wandering, the results show the suction peak increases in magnitude on the upper surface as the blade incidence is increased. Further, a clear maximum is observed at $\alpha = 6$ deg. This maximum in suction peak also occurs at the same incidence setting for transducer locations farther downstream. With the blade incidence set below $\alpha = -4$ deg, the mean value in suction peak is reduced (compared with $\alpha = 0$ deg) and remains relatively constant.

Once the upper-surface suction ridge has moved aft of approximately 15% chord, it increases in strength at $\alpha = 4$ deg but diminishes at $\alpha = 10$ deg. Also, with increasing negative incidence, the ridge becomes weaker until it is insignificant at $\alpha = -10$ deg.

On the lower surface, the change in incidence has a similar effect on the observed pressure pulse. As the incidence is increased in the positive sense (Figs. 7a and 7b), the pressure pulse is reduced. When the incidence becomes negative (Figs. 7c and 7d), the pressure pulse at the leading edge increases in magnitude. In Fig. 9, the peak pressure results from 20 orthogonal vortex interactions have been extracted from a transducer on the lower surface and near the leading edge $(x/c = 0.011)$. An increase in pressure pulse magnitude [denoted by a decrease in $(C_{pu} - C_{ps})$] with decreasing incidence can be observed from the results. The general form of the curve is monotonic, except at negative incidence values beyond $\alpha = -5$ deg. It is interesting to note that, in this respect, this behavior is almost a mirror image of that presented in Fig. 8. In Fig. 9, each data point represents a mean value, with the error bars indicating one standard deviation.

Common to all surface pressure records is the sudden application of suction to the upper surface and pressure to the lower surface in the region of the leading edge. This behavior is thought to be due to the cross-flow velocity within the core, assumed to be the axial flow component. This flow is directed toward the lower surface and away from the upper surface. Hence, the observed pressure signatures are similar to those obtained by the impulsive blocking of an incompressible jet.

The amplification and attenuation of the initial suction and pressure peaks as the incidence is changed are interesting phenomena; however, a straightforward explanation of the results is, at this stage, unavailable. They possibly result from the interaction of the blade leading edge with cross-stream velocity components of the

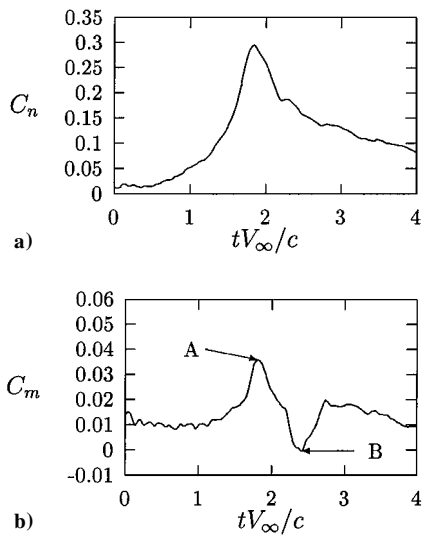

Fig. 11 (a) Normal force and (b) quarter chord pitching moment data; $\alpha = 0$ deg.

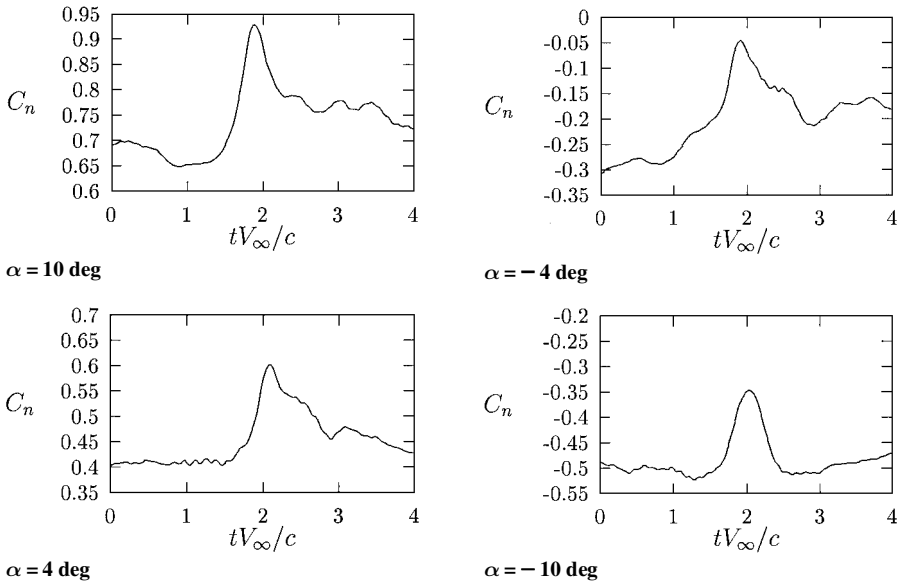

Fig. 12 Normal force measurements on loaded blade.

approaching vortex and the action of the leading-edge boundary layer being entrained into the low-pressure vortex core. Also, the fact that the peak suction and pressure magnitudes show some disturbance beyond $\alpha = \pm 5$ deg indicates that some change in the flow environment occurs at higher incidence. Further experiment and modeling are required to increase the understanding of the vortex collision fluid dynamics at the leading edge.

On the lower surface, the pressure ridge is seen to transform into a slight suction ridge after the vortex passes approximately 15% of the chord. This process can be viewed in more detail by observing the individual pressure records on the lower surface for the case where $\alpha = 0$ deg (Fig. 10). The suction ridge begins very close to the leading edge as a small disturbance (denoted by the symbol * in Figs. 10a and 10b) that appears before the arrival of the main pressure pulse. This small disturbance grows in magnitude as the pressure pulse attenuates until it eventually evolves into the weak suction ridge. This behavior is difficult to explain but may indicate the development of secondary vorticity on the lower surface. Physically, this would be due to the interaction of the vortex velocity components with the blade boundary layer, initiating a small region of localized separation.

Secondary vorticity may also develop on the upper surface; however, it would be obscured by the already strong suction ridge around the leading edge. The production of this strong suction ridge is expected, as the low pressure within the vortex core will act together with the transient low pressure initiated by the cutting of the cross-stream velocity component.

The surface pressure records were integrated to obtain normal force and quarter-chord pitching moment coefficients (per unit span). This was done by assuming that the pressure varied linearly between transducer locations at each sample point in time. This pressure distribution was then integrated around the blade using standard trapezoidal integration routines that approximated the normal force and pitching moment integrals. The pressure was extrapolated to the trailing edge by using the slope of the pressure distribution from the two transducers closest to the trailing edge.

Figure 11 shows these results for the case where incidence was set at $\alpha = 0$ deg. The normal force rapidly increases as the vortex collides with the blade and then decreases as the vortex passes over the rest of the surface. The rapid rise in force is likely to be due to the impact of the core axial component with the leading edge. If this component was not present, then an equal loading distribution would be expected about the blade and no net normal force would arise. Immediately after the interaction with the rotor tip vortex, the blade is immersed in an unsteady vortex sheet created by the inboard portion of the rotor blade. This vortex sheet will induce additional forces on the blade that lead to the asymmetry observed in the results.

Figure 11b shows the quarter-chord pitching moment during the orthogonal vortex interaction. The blade experiences a rapid nose-up pitching moment as the vortex passes over the leading edge. The value of the pitching moment then falls as the vortex passes over the blade, before reestablishing itself at the preinteraction level as the vortex passes beyond the trailing edge. Although the suction peak on the upper surface is small only over the trailing edge, the moment arm is long; hence the significant effect on the pitching moment.

Normal force results for the blade at a selection of incidence settings are shown in Fig. 12. In each figure, the relative range of the vertical axes remains the same; however, each is offset by a different amount due to the static loading on the blade at each incidence setting. Each record shows a sharp rise in magnitude as the vortex collides with the blade in a manner similar to the case at $\alpha = 0$ deg. The unsteadiness that occurs after the main interaction is associated with the vortex sheet discussed earlier.

Figure 13 shows the variation in peak normal force measured during the interaction over the range of incidence settings used in the experiments. The plotted value ΔC_n is the difference between the peak and time-averaged normal force coefficients. Therefore, ΔC_n represents the impulsive normal load imparted to the blade by the interaction of the vortex only, with the offset of the steady aerodynamics removed. Each data point in Fig. 13 represents the mean of 20 vortex interactions, and the error bars indicate the standard deviation. The results show that, as the blade incidence is changed, the impulsive peak normal force experienced by the blade is approximately the same. Recent normal force measurements taken during a simulated main rotor BVI[2] indicate a similar result despite the fact that the vortex interaction is of a different type.

For the results presented here, it is thought that the peak magnitude in normal force is maintained due to the amplification and attenuation of suction and pressure peaks around the leading edge at different incidence settings. At positive incidence, the suction

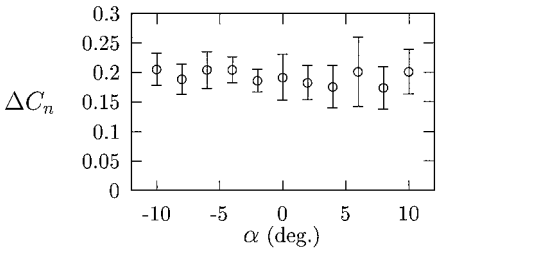

Fig. 13 Variation of ΔC_n with blade incidence.

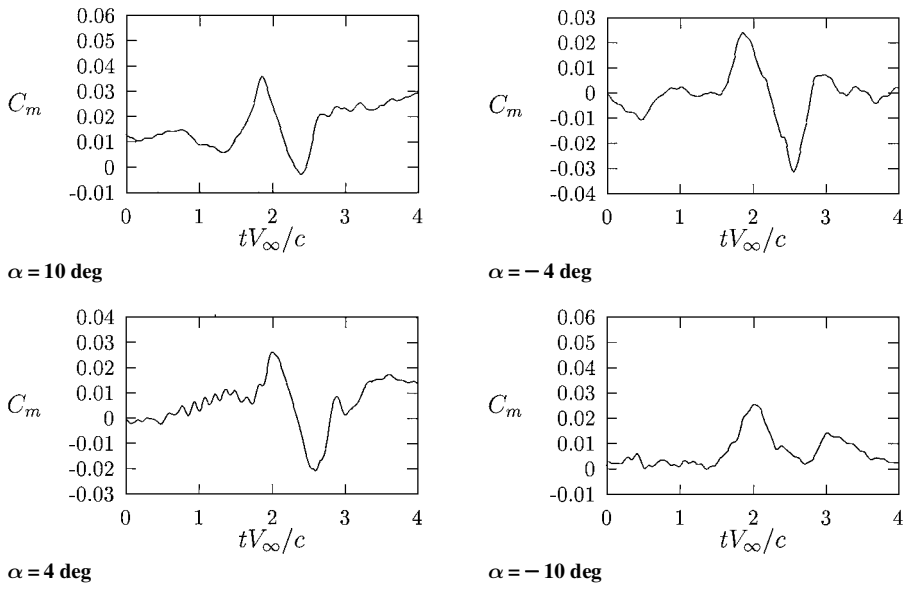

Fig. 14 Quarter chord pitching moment measurements on loaded blade.

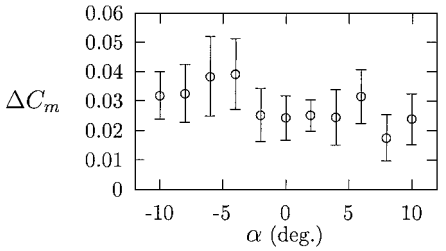

Fig. 15 Variation of ΔC_m with blade incidence.

peak is increased while the pressure pulse is reduced, and the opposite is true at negative incidence. Therefore, even if the upper and lower surface pressure distributions are altered, the overall effect on transient normal force is the same.

Similarly, the quarter-chord pitching moment results (Fig. 14) are similar in form to those of the unloaded case, showing the rapid increase as the vortex collides with the blade, followed by a reduction and subsequent recovery as the vortex moves over the chord. Figure 15 plots the change in pitching moment ΔC_m against blade incidence. The value ΔC_m is defined as the difference between the maximum and minimum quarter chord pitching moment levels during the interaction. The locations of maximum and minimum pitching moment are identifed as points A and B respectively in Fig. 11, and the error bars in Fig. 15 indicate one standard deviation. Although there is some change in ΔC_m with incidence, it is difficult to see a trend, due to the sensitivity of the pitching moment to vortex wandering.

Conclusions

Experimental results obtained during a series of tests that investigated the orthogonal vortex interaction with an instrumented stationary blade under different loading conditions, were presented.

These experiments were performed in two parts. The first involved a study of the vortex system using hot wire anemometry and PIV. This showed that a well-defined, three-dimensional vortex was available for the orthogonal interaction with the blade. Hot wire anemometry allowed velocity measurements within the core. However, these were susceptible to the effects of vortex wandering. Measurements taken with the PIV system overcame these problems, but seeding difficulties prohibited quantification of details within the vortex core itself. Despite these difficulties, integration of the PIV results several core diameters away from the core still allowed determination of vortex total circulation.

The second part of the experiments used a single, instrumented blade to study the interaction over a range of different incidence settings. In all cases, the upper surface of the blade experienced a strong suction peak and the lower surface a pressure pulse as the vortex collided with the leading edge. Flowfield measurements indicated that the vortex contained a significant axial core flow that was directed toward the lower surface and away from the upper surface. The results around the leading edge during vortex collision are therefore analogous to the sudden blocking of an incompressible jet and qualitatively agree with the results of other researchers.[5–8] A weak instability on the lower surface developed on the leading edge, which later transformed into a small suction ridge over the remainder of the chord. This disturbance may indicate the development of secondary vorticity in the blade-boundary layer due to a small region of localized separation underneath the vortex.

Transient normal-force data showed a rapid rise as the vortex impacted with the leading edge. Simultaneously, as the vortex moved off the blade surface, the quarter chord pitching moment data exhibited a nose-up moment followed by a rapid reduction in magnitude before re-establishing itself at the pre-interaction level.

As the incidence was changed, the pressure reactions at the blade-leading-edge were amplified or attenuated, depending on the sense of the incidence setting. Further, the changes in pressure distribution occurred in such a way that the magnitude of the peak normal force coefficient remained approximately the same for all incidence cases tested. These changes in pressure distribution with incidence were likely influenced by the interaction of the axial core flow and the leading edge boundary layer.

Acknowledgments

This work was funded by the Engineering and Physical Sciences Reseach Council, the Defence Evaluation and Research Agency, Farnborough, and GKN-Westland Helicopters, Ltd., under Grant GR/L 58231. The authors would also like to thank R. Green for the PIV images, C. Copland for the design of the vortex generator rig, and R. Gilmour and D. Perrins for their technical assistance.

References

[1]Straus, J., Renzoni, P., and Mayle, R., "Airfoil Pressure Measurements During a Blade-Vortex Interaction and Comparison with Theory," *AIAA Journal*, Vol. 28, No. 2, 1990, pp. 222–228.

[2]Masson, C., Green, R., Galbraith, R., and Coton, F., "Experimental Investigation of a Loaded Rotor Blade's Interaction with a Single Vortex," *Aeronautical Journal*, Vol. 102, No. 1018, 1998, pp. 451–457.

[3]Conlisk, A., "A Theory of Vortex-Surface Collisions," AIAA Paper 98-2858, June 1998.

[4]Howe, M., "On Unsteady Surface Forces, and Sound Produced by the Normal Chopping of a Rectilinear Vortex," *Journal of Fluid Mechanics*, Vol. 206, 1989, pp. 131–153.

[5]Marshall, J., "Vortex Cutting by a Blade, Part 1: General Theory and a Simple Solution," *AIAA Journal*, Vol. 32, No. 6, 1994, pp. 1145–1150.

[6]Marshall, J., and Yalamanchili, R., "Vortex Cutting by a Blade, Part 2: Computations of Vortex Response," *AIAA Journal*, Vol. 32, No. 7, 1994, pp. 1428–1436.

[7]Lee, J., Burggraf, O., and Conlisk, A., "On the Impulsive Blocking of a Vortex Jet," *Journal of Fluid Mechanics*, Vol. 369, 1998, pp. 301–331.

[8]Marshall, J., and Krishnamoorthy, S., "On the Instantaneous Cutting of a Columnar Vortex with Non-Zero Axial Flow," *Journal of Fluid Mechanics*, Vol. 351, 1997, pp. 41–74.

[9]Krishnamoorthy, S., and Marshall, J., "Three-Dimensional Blade Vortex Interaction in the Strong Vortex Regime," *Physics of Fluids*, Vol. 10, No. 11, 1998, pp. 2828–2845.

[10]Cary, C., "An Experimental Investigation of the Chopping of Helicopter Main Rotor Tip Vorticies by the Tail Rotor. Part II: High Speed Photographic Study," NASA Contractor Rept. 177457, Sept. 1987.

[11]Ahmadi, A., "An Experimental Investigation of Blade-Vortex Interaction at Normal Incidence," *AIAA Journal*, Vol. 23, No. 1, 1986, pp. 47–55.

[12]Johnston, R., and Sullivan, J., "Unsteady Wing Surface Pressures in the Wake of a Propeller," AIAA Paper 98-0277, June 1998.

[13]Doolan, C., Coton, F., and Galbraith, R., "Three-Dimensional Vortex Interactions with a Stationary Blade," *Aeronautical Journal*, Vol. 103, No. 1030, 1999, pp. 579–587.

[14]Copland, C., "Methods of Generating Vortices in Wind Tunnels," Ph.D. Dissertation, Dept. of Aerospace Engineering, Univ. of Glasgow, Glasgow, Scotland, U.K., 1997.

[15]Green, R. B., Doolan, C. J., and Cannon, R. M., "Measurements of the Orthogonal Blade-Vortex Interaction Using a Particle Image Velocimetry Technique," *Experiments in Fluids*, Vol. 29, 2000, pp. 369–379.

[16]Doolan, C., Coton, F., and Galbraith, R., "Measurement of Three-Dimensional Vortices Using a Hot Wire Anemometer," AIAA Paper 99-3810, June–July 1999.

[17]Baines, N., Mee, D., and Oldfield, M., "Uncertainty Analysis in Turbomachine and Cascade Testing," *International Journal of Engineering Fluid Mechanics*, Vol. 4, No. 4, 1991, pp. 375–401.

[18]Han, Y., Leishman, J., and Coyne, A., "Measurements of the Velocity and Turbulence Structure of a Rotor Tip Vortex," *AIAA Journal*, Vol. 35, No. 3, 1997, pp. 477–485.

[19]Leishman, J., "Seed Particle Dynamics in Tip Vortex Flows," *AIAA Journal*, Vol. 33, No. 4, 1996, pp. 823–825.

[20]Devevport, W. J., Rife, M. C., Liapis, S. I., and Follin, G. J., "The Structure and Development of a Wing-Tip Vortex," *Journal of Fluid Mechanics*, Vol. 312, 1996, pp. 67–106.

M. Samimy
Associate Editor